Ferroelectrics, 2001, Vol. 236, pp. 129-144
Reprints available directly from the publisher
Photocopying permitted by license only

Regular Ferroelectric Domain Array in Lithium Niobate Crystals for Nonlinear Optic Applications

V.YA. SHUR[a], E.L. RUMYANTSEV[a], E.V. NIKOLAEVA[a], E.I. SHISHKIN[a], R.G. BATCHKO[b], G.D. MILLER[b], M.M. FEJER[b] and R.L. BYER[b]

[a]*Ural State University, 620083 Ekaterinburg, Russia and* [b]*E.L. Ginzton Lab, Stanford University, Stanford, CA 94305*

(Received July 12, 1999)

We present our experimental investigations of the domain evolution in lithium niobate. Particular attention is paid to the short-pitch and nanoscale domain patterning. We demonstrate the production of domain patterns with period down to 2.6 μm in 0.5-mm-thick $LiNbO_3$ wafers by backswitched poling using lithographic stripe electrodes and nanoscale domain patterns consisting of strictly oriented arrays of nanodomains (diameter down to 30 nm, density up to 100 μm^{-2}).

Keywords: domain structure; backswitching; domain engineering; kinetics; switching; nanotechnology.

INTRODUCTION

In recent years rapid development of a new branch of technology named the microdomain engineering raised the questions of fabrication of ferroelectric domain patterns with periods about several microns. The solving of this problem is a critical step in the improvement of characteristics of electro-optical [1] and nonlinear optical device.[2] The

new class of engineerable nonlinear optical materials is widely used for the development of wide range of tunable coherent light sources based on quasi-phase matching.[3] Lithium niobate $LiNbO_3$ (LN) is one of the most important representatives of this class due to large electro-optical and nonlinear optical coefficients.[4] The new method based on the application of electric field through lithographically defined electrodes for domain patterning allows the production of available devices for wide usage.[5] However the extremely high coercive voltage and the impeding effect of domain spreading out of the electroded area impose problems in obtaining the short-pitch domain patterns. In this work we report the results of an experimental study which allows this obstacle to be overcome. Moreover, we present the first results on nanoscale domain engineering. The knowledge of the physical principles of the formation of "super-short" domain patterns in thick wafers of such "inconvenient" material as "the frozen ferroelectric"[4] LN opens wide perspectives in other ferroelectrics.

EXPERIMENT

The periodic domain structures were prepared in optical-grade single-domain 0.5-mm-thick LN wafers of congruent composition cut perpendicular to polar axis. The wafers were photolithographically patterned with periodic strip metal (NiCr) electrodes deposited on $\mathbf{Z}^+$ surface and oriented along the **Y** axis. The patterned surface was covered by a thin (about 0.5-μm thick) insulating layer (photoresist) (Fig. 1a).

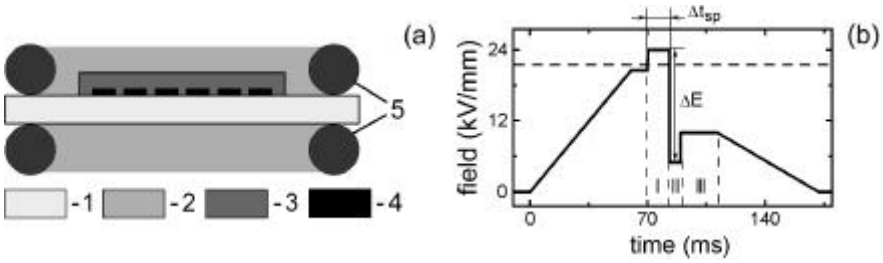

FIGURE 1 Scheme of experimental setup (a) and voltage waveform (b). 1 - lithium niobate wafer, 2 - liquid electrolyte (LiCl), 3 - insulating layer, 4 - metal electrodes, 5 - O-rings.

A high voltage pulse producing an electric field greater than the coercive field (E_c = 21.5 kV/mm) was applied to the structure through the fixture containing a liquid electrolyte (LiCl).[6,7] The waveform for backswitched poling consisted of three levels of external field: "high field", "low field" and "stabilization field" (Fig. 1b).

The switching from single domain state took place at "high field" and the backswitching (flip-back) [8-10] occurred at "low field". The crucial parameters for backswitching kinetics were the duration of the "high field" stage Δt_{sp} and the field diminishing amplitude ΔE. The domain patterns obtained for the different duration of the "low field" stage yielded information about the domain structure development during backswitching. For observation of the domain patterns after partial poling **Z** surfaces and polished **Y** cross-sections were etched for 5-10 min by hydrofluoric acid without heating.[7] The surface relief obtained was visualized by optical microscope, SEM and AFM techniques.

Moreover we carried out direct observations of the domain evolution using a polarizing microscope with simultaneous TV recording and image processing. We investigated 0.2 mm-thick wafers of LN with liquid electrolyte electrodes on both sides. This technique allows direct information to be obtained about the reconstruction of the domain shape and to obtain the field dependence of the sideways wall motion velocity, which is of principal importance for optimization of the poling voltage waveform.

MAIN STAGES OF THE DOMAIN EVOLUTION

In our recent papers [8-10] it was shown that the domain evolution during backswitched poling undergoes distinct stages (Fig. 2).

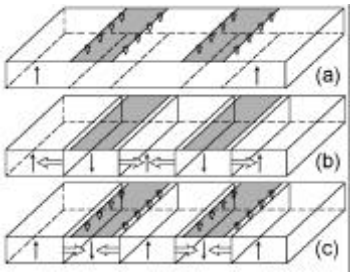

FIGURE 2 The main stages of domain evolution during switching in single domain plate with stripe electrodes.

The first switching stage is the nucleation (arising of new domains) and formation of arrays of isolated domains at **Z+** polar surface along the electrode edges. This starts at the beginning of the "high field" stage (Fig. 2a). At the second switching stage, the nucleated domains grow and merge under the electrodes and the laminar domains formed spread out of electroded area (Fig. 2b). During the backswitching stage, which begins after rapid field decreasing (the "low field" stage), shrinking of the laminar domains by backward wall motion and nucleation along the electrode edges occurs (Fig. 2c). We controlled the domain kinetics at each stage by the choice of the voltage waveform parameters. Short-pitch domain patterns of high fidelity and nanodomain structures have been produced by backswitched poling.

MAIN APPROACH

Our approach to domain patterning is based on understanding of key role of bulk screening effects.[11,12] It is well known that polarization reversal from the single domain state is achieved by nucleation of new domains and their growth.[13,14] Both processes are governed by the elementary nucleation at the domain wall (domain growth) and far from the wall (nucleation/arising of new domains). The local electric field E_s averaged over the volume of nuclei is the driving force of both these processes.[11,14] The local field $E_s(r,t)$ is determined by the sum of external field $E_{ex}(r)$, the depolarization field $E_{dep}(r,t)$ produced by bound charges, and the screening fields due to the charge redistribution at the electrodes – the external screening field $E_{escr}(r,t)$ and in the bulk – the bulk screening field $E_{bscr}(r,t)$ [14-16]

$$E_s(r,t) = E_{ex}(r) - [E_{dep}(r,t) - E_{escr}(r,t) - E_{bscr}(r,t)] \qquad (1)$$

The depolarization field slows the domain growth while the screening process reduces its influence. After complete external screening the bulk residual depolarization field E_{dr} remains due to the surface dielectric gaps of the thickness L [14,16]

$$E_{dr} = E_{dep} - E_{escr} = 2L\, P_S\, (\varepsilon_L \varepsilon_o d)^{-1} \qquad (2)$$

where P_S - spontaneous polarization, ε_L - dielectric permittivity of the gap.

This residual field can be screened by the charge redistribution in the bulk, injection through the insulating layer and/or aligning of polar

defects.[15,16] After removing of the external field the spontaneous backswitching process is obtained if

$$E_s(r,t) = -[E_{dep}(r,t) - E_{escr}(r,t) - E_{bscr}(r,t)] > E_{th} \qquad (3)$$

Thus the initial single domain state can be even completely reconstructed. So the understanding of the screening effects is crucial for control backswitching which had been used to enhance the fidelity of fine-pitch domain structures.

Nucleation under the electrode edges

In order to explain the nucleation and formation of the arrays under the electrode edges, the spatial distribution of the polar component of the switching field $\mathbf{E_Z}$ produced in a periodically electroded sample was calculated (Fig. 3). This distribution demonstrates sharp singularities under the electrode edges. The spatially nonuniform $\mathbf{E_Z}(x,y)$ exists only in the vicinity of the surface and its amplitude rapidly decreases with the depth (Fig. 3). Practically uniform field is obtained at a depth more than electrode period. Such estimations clarify the cause of spatially nonuniform nucleation in thin surface layer and show that subsequent growth of domains in the bulk goes on in uniform field.

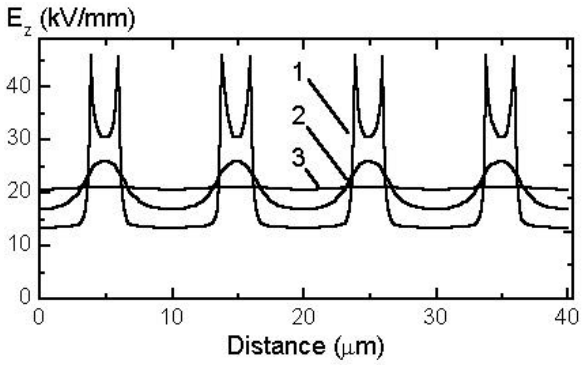

FIGURE 3 Calculated spatial distribution of field polar component E_Z near $\mathbf{Z^+}$ surface of periodically electroded sample.

The switching current data give additional information about the nucleation and forward growth processes (Fig. 4). The duration of two important steps of domain evolution can be obtained. Up to $\mathbf{t_1}$ current is proportional to $\mathbf{t^2}$, which corresponds to the growth of isolated domains arising with constant nucleation rate (α process)

along electrode edges. Thus $\mathbf{t_1}$ is the moment when independently growing isolated domains start to merge. $\mathbf{t_1} = 0.5\ \mathbf{Dy}/\mathbf{v_s}$, where **Dy** - the average distance between nuclei, $\mathbf{v_s}$ - velocity of sideways domain growth under the electrode edges. At $\mathbf{t_2}$ the first domains reach $\mathbf{z^-}$ as a result of forward growth (tip propagation) with velocity $\mathbf{v_f}$. $\mathbf{t_2} = \mathbf{d}/\mathbf{v_f}$. The knowledge of $\mathbf{t_1}$ and $\mathbf{t_2}$ allows determination of the averaged tip propagation rate 304 ± 29 mm/s and sideways domain wall motion velocity of small isolated domains 0.51 ± 0.04 mm/s.

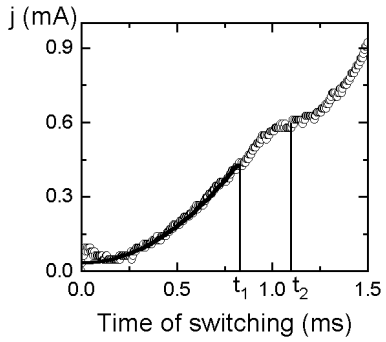

FIGURE 4 Switching current corresponding to growth and merging of isolated domains under the electrode edges.

Correlated nucleation

There is much evidence for spatial correlated nucleation during switching in LN in uniform field. One of the common manifestations is the nucleation at a short distance from a domain wall (Fig. 5). Correlated nucleation plays an important role during backswitching.

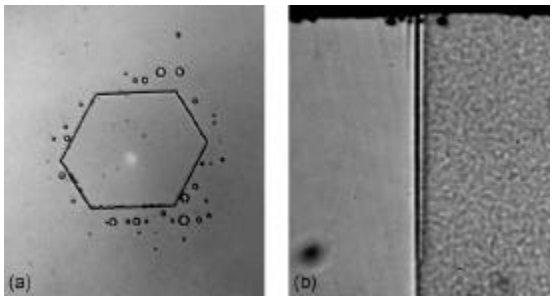

FIGURE 5 Formation of nuclei near the domain wall. (a) **Z** view, (b) **Y** view. Domain patterns were revealed by etching and visualized by optical microscope.

In the framework of our approach, correlated nucleation is due to the peculiarities of the spatial distribution of $\mathbf{E_z}$ near the wall because of the existence of an intrinsic dielectric gap. The results of our calculations of the field distribution produced by an individual stripe encountering a domain located at the surface in an infinite plate completely covered by uniform electrodes is presented in Fig. 6. It is seen that the field maxima are situated at a distance of about the thickness of the dielectric gap **L** from the wall (Fig. 6).

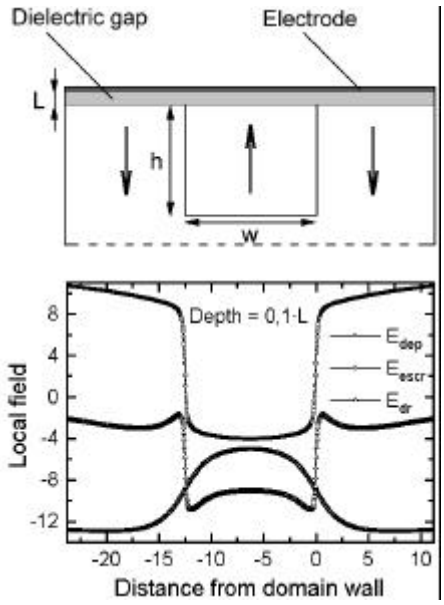

FIGURE 6 Scheme of the surface layers (a) and spatial field distribution (b) caused by stripe domain. Distance and depth are given in units of gap thickness L.

This calculation shows that maxima of local field determining the position of the nucleation site exist only near the surface and disappear at the depth of the order of **L**.

Domain frequency multiplication during backswitching

The investigation of domain kinetics during backswitching revealed a new effect - multiplication of the domain pattern frequency as compare to the electrode one.[17] The mechanism of the multiplication is based on the aforementioned correlated nucleation. Different variants of multiplication can be obtained by varying the width of electrodes and domains formed during switching (Fig. 7).

"Frequency doubling" can be obtained as a result of the appearance of additional backswitched stripe domains under the whole electrode on $\mathbf{Z}^+$ (Fig. 7a,b). The depth of backswitched domains depends on the electrode width and is about 50 - 100 μm.

"Frequency tripling" was achieved through arising of additional domain "strips" with depth about 20 - 50 μm under electrode edges using wider electrodes and a shorter backswitching stage (Fig. 7c,d).

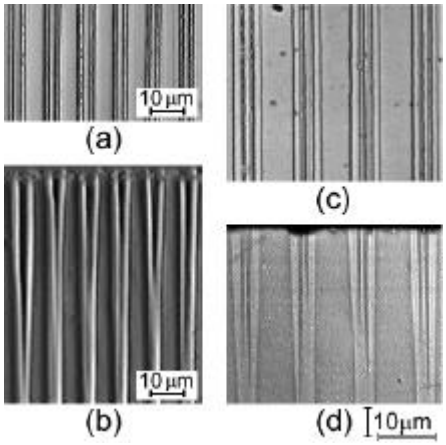

FIGURE 7 "Frequency doubling": $\mathbf{Z}^+$ (a) and **Y** (b) view. "Frequency tripling": $\mathbf{Z}^+$ (c) and **Y** (d) view.

Image processing of tilted cross-sections demonstrates the strong correlation in spatial distribution of domains in the arrays arisen during "frequency doubling". The average distance between nuclei was found to be 0.91±0.04 μm (Fig. 8) and depth - 52 ± 6 μm.

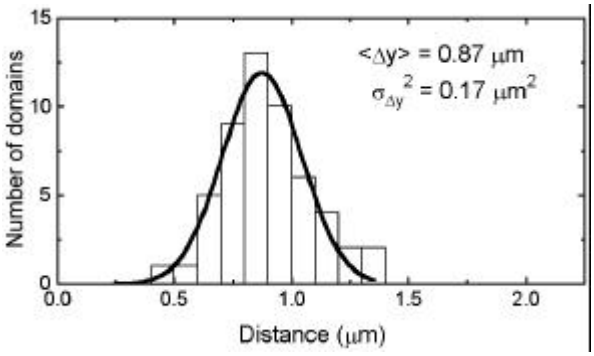

FIGURE 8 Histogram of the distances between the neighboring domains fitted by the normal distribution.

DOMAIN SPREADING

In order to investigate domain spreading out of the electroded area we use direct optical observation of the domain evolution during switching using only liquid electrodes on both surfaces. The typical domain structure evolution in this case is the nucleation along the electrode edges and propagation of the formed domain walls to the center. For detailed visualization of the starting stages of domain evolution we choose a place on the crystal surface with a small scratch (playing a role of the array of nucleation sites) in the center of the switched area.

The domain walls are mostly oriented along **Y** directions and any instantaneous local deviation from the allowed crystallographic orientations rapidly disappears. It can be seen that the domain growth is connected with the propagation of microscale domain steps along the wall (Fig. 9).

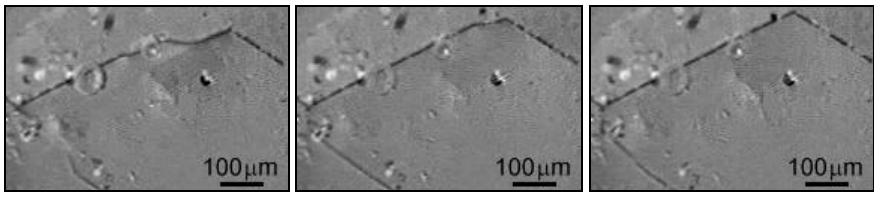

(a) (b) (c)

FIGURE 9 Layer-by-layer growth through step propagation along the wall during repoling in uniform field. Time interval between the sequent frames 2 s, E = 15.3 kV/mm.

The fastest step of the domain evolution is connected with transformation from concave domain shape (forming as a result of merging) to the regular convex one. The typical scenario of the "gulping" of small domain by the big one is demonstrated at the Figure 10.

Moreover it must be stressed that the "prints" of the domain wall are observed after the wall shift (Fig. 10). A similar effect was obtained in lithium tantalate.[18] These prints gradually disappear during a time of about one second. The prints appear only at the places where the wall was staying for a long enough time (more than second) and the print lifetime is proportional to this time.

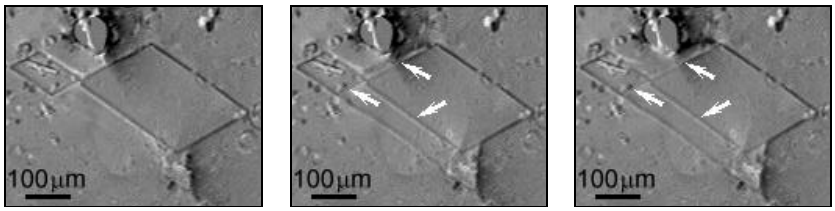

(a) (b) (c)

FIGURE 10 "Gulping" during repoling in uniform field. Arrows indicate the prints of the domain walls. Time interval between the sequent frames 40 ms, E = 15.3 kV/mm.

In situ observations of the domain kinetics allow the determination of the field dependence of the average sideways wall motion velocity by a direct method (Fig. 11). It is found a the conventional field dependence is observed in a wide range of velocities (threshold field for poling 17.8 kV/mm and for repoling 14.0 kV/mm)

$$V(E) = V_\infty \exp[E_{ac}/(E - E_{th})] \qquad (4)$$

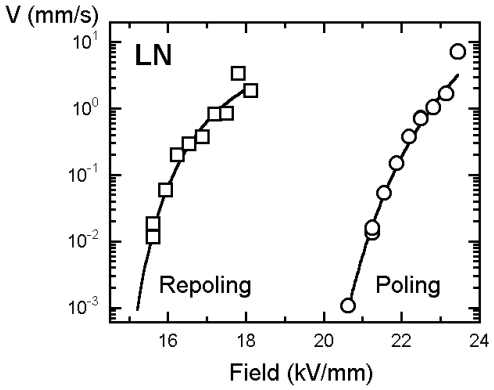

FIGURE 11 Field dependence of the average velocity of domain wall motion. Experimental points are fitted by Equation (4).

FORMATION OF NANODOMAINS DURING BACKSWITCHING

We have discovered that if the switching process is accompanied by a sufficient spreading of domain walls out of the electrodes the evolution of domains during backswitching is a highly organized process.[19] The spontaneous decay of metastable structure existing after removing of external field proceeds through arising and growth of oriented nanoscale domain arrays contrary to the expected trivial

reversal motion of existing domain walls accompanied by random nucleation of new domains. There exist two main limiting scenarios of domain evolution under various backswitching conditions

Formation of periodic strip domains along the electrode edges

For the high field-diminishing amplitude **DE** ~ 20 kV/mm and long switching pulse $\mathbf{Dt_{sp}}$ ~ 15 ms (Fig. 1b) the backswitching starts with formation of a pair of 1D-nanodomain arrays strictly under the electrode edges (Fig. 12a). At the second stage of domain evolution the arrays turn into a pair of strip domains through growth and merge of nanodomains (Fig. 12b). Surprisingly, after complete merging the new pair of 1D arrays appears in nonelectroded area parallel to the first ones (Fig. 12c).

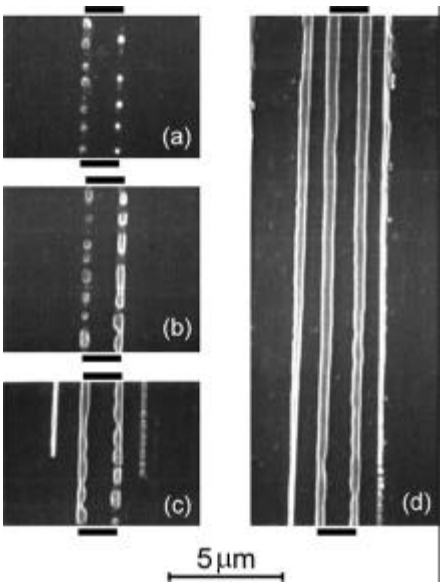

FIGURE 12 SEM patterns demonstrating the stages of the formation of periodic strip domains along the electrode edges. Black rectangles show the position of the electrodes.

This self-maintaining process leads to formation of periodic strip domains oriented along the electrodes (Fig. 12d).

In this case, the pulse duration is long enough to ensure the reorientation of the bulk screening field and essential bulk screening of the external field. So an additional backswitching field proportional to **DE** remains after field diminishing. The calculated spatial distribution

of the field polar component in the surface layer (Fig. 13a) is presented in Fig. 13b. The positions of obtained field maxima define the positions of the first arrays of nanoscale domains (Fig. 12a). The observed correlated distribution of nanodomains along array is due to the electrostatic nuclei-nuclei interaction resulted from peculiarities of field distribution near the walls discussed above.

The growth and merging of nanodomains of the first arrays change the field distribution. Calculations show that a new backswitching field maximum appears at a distance of about the thickness of the insulating layer from the array (Fig. 12c). Field anomalies determine the position of the second array couple, which is confirmed experimentally.

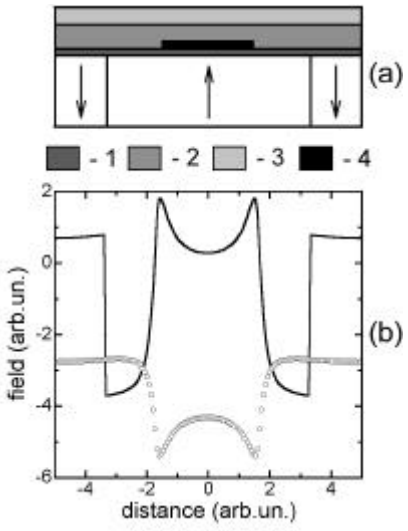

FIGURE 13 (a) Scheme of sample surface region with stripe electrode: 1 - dielectric gap, 2 - insulating layer, 3 - liquid electrolyte, 4 - metal electrode. (b) Calculation of spatial distribution of backswitching field near surface in limiting cases (line - low ΔE and short Δt_{sp}, points - high ΔE and long Δt_{sp}).

Formation of self-organized nanodomain structures

For the low field-diminishing amplitude $\mathbf{DE}$ ~ 2 kV/mm and short switching pulse duration $\mathbf{Dt_{sp}}$ ~ 5 ms the domain patterns demonstrate arising and propagation of a highly organized quasi-periodical structure of domain arrays strictly oriented along one of the $\mathbf{Y^-}$ directions at 60 degrees to the electrode edges (Fig. 14a). Each array

is comprised of nanodomains with diameter 30-100 nm and average linear density exceeding 10^4 mm^{-1}. In some cases domain arrays are oriented along **X** directions at 30 and 90 degrees to the electrode edges (Fig. 14b). The 90 degree arrays organize periodical set of stripe domains with period down to 60 nm along the existing wall (Fig. 14c).

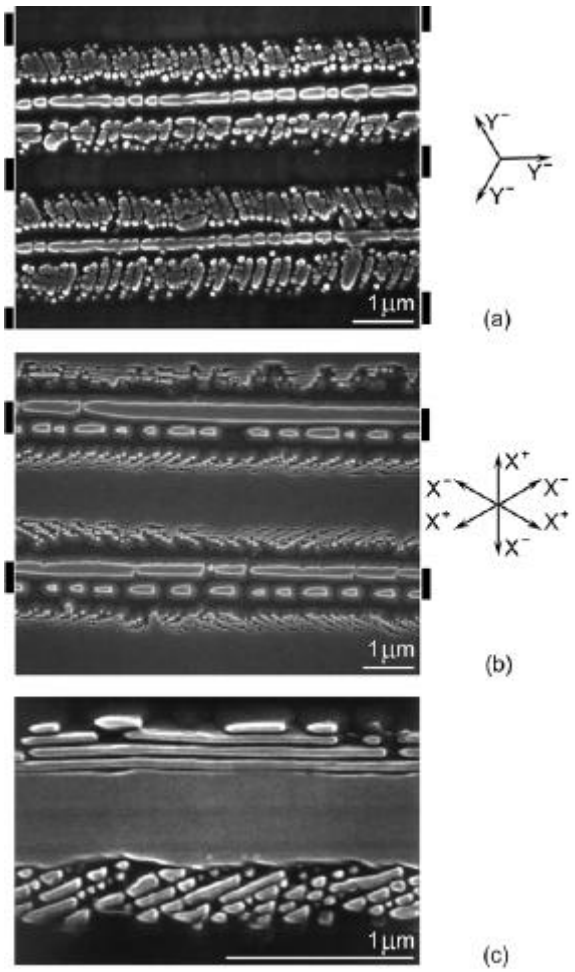

FIGURE 14 Nanodomain arrays oriented along $\mathbf{Y}^-$ directions at 60 degrees (a), along **X** directions at 30 degrees (b). Domain patterns revealed by etching were visualized by SEM. Black rectangles show the electrode position.

For array-assisted growth the low value of **DE** excludes the influence of field singularities at the electrode edges. It is seen from Fig. 13b that the backswitching field abruptly increases while moving away from the walls, slightly varies in the nonelectroded area and smoothly decreases to the electroded edges. The array-assisted growth develops in the region of strong depolarization field. The orientation of arrays strictly along crystallographic directions is evidence of a strong influence of crystal anisotropy on the nucleation kinetics.

The simultaneously developing process of correlated nucleation represents the self-maintaining generation of the parallel arrays. This effect is of the same origin as the above-discussed array formation along the electrode edges (Fig. 12). The existing array aggregate generates a new maximum of backswitching field at a fixed distance in front of its boundary and triggers arising of a new array. Such self-maintaining growth leads to "super-fast" polarization reversal by the fast spreading of ordered structure consisting of the oriented arrays of nanodomains. The array-assisted propagation of the domain structure is similar to the formation of “the wide domain boundary” discovered in $Pb_5Ge_3O_{11}$ during switching in "super-strong" fields.[20] Avalanche nucleation leads to the enhancing of the propagation velocity of the switching area, which may exceed the sound velocity. Such an effect can manifest itself during superfast switching, thus explaining the nanosecond range switching kinetics in ferroelectric thin films.

Quasy-phase-matched second harmonic generation in backswitched poled LN

Continuous-wave single-pass second harmonic generation was obtained in 4-μm-period 0.5-mm-thick backswitched-poled LN.[21] Pump sources at 920-930 nm include both Ti:S and diode-oscillator-amplifier lasers. Second harmonic generation of Ti:S laser at 6.1 %/W efficiency, producing 61 mW at $\mathbf{l}$ = 460 nm, was demonstrated in 50-mm-length periodically poled LN samples having a nonlinear coefficient $\mathbf{d_{eff}} \approx 9$pm/V, while 60 mW at 465 nm and 2.8-%/W efficiency was obtained by second harmonic generation of a laser diode source.[21]

CONCLUSIONS

We have analyzed the main stages of domain patterning in LN. The domain evolution during backswitching after removing of the poling

field was investigated for the first time. The important role of backswitching as a powerful tool for producing short domain patterns has been demonstrated. We have reported the first observation of experimental evidence of self-organizing decay of the highly nonequilibrium ferroelectric domain structure in LN through formation of ordered nanodomain arrays. It must be pointed out that formation of the nanoscale domains is the only mechanism of polarization reversal without screening. As a result the propagation velocity of the spike-like nanodomains area is much faster then sideways motion velocity of the domain walls. The obtained results can help in explanation of the nanosecond range switching kinetics in thin films.

ACKNOWLEDGMENTS

This paper is based upon work partially supported by the Program "Basic Research in Russian Universities" under Grant No.5563, by the EOARD, Air Force Office of Scientific Research, AFRL, under Contract No.F61775-99-WE037 and by DARPA/ONR through the Center of Nonlinear Optical Materials at Stanford University under ONR Grant No.00014-92-J-1903 and LLNL.

REFERENCES

1. M. Yamada, M. Saitoh, and H. Ooki, *Appl.Phys.Lett*., **69**, 3659 (1996).
2. R.L. Byer, *J. Nonlinear Optic. Phys. & Mater*., **6**, 549 (1997).
3. K.C. Burr, C.L. Tang, M.A. Arbore, and M.M. Fejer, *Appl. Phys. Lett*., **70**, 3343 (1997).
4. A.M. Prokhorov and Y.S. Kuzminov, *Physics and Chemistry of Crystalline Lithium Niobate* (Adam Hilger, Bristol, 1990), p.263.
5. M. Yamada, N. Nada, M. Saitoh, and K. Watanabe, *Appl. Phys. Lett*., **62**, 435 (1993).
6. L.E. Myers, R.C. Eckardt, M.M. Fejer, R.L. Byer, and W.R. Bosenberg, *Optic Lett.*, **21**, 591 (1996).
7. G.D. Miller, R.G. Batchko, M.M. Fejer, and R.L. Byer, *SPIE Proc. on Solid State Lasers and Non-linear Crystals*, **2700**, 34 (1996).
8. V.Ya. Shur, R.G. Batchko, E.L. Rumyantsev, G.D. Miller, M.M. Fejer, and R.L. Byer, *Proc. 11th ISAF, Piscataway, NJ: IEEE*, 399 (1999).

9. V. Shur, E. Rumyantsev, R. Batchko, G. Miller, M. Fejer, and R. Byer, *Ferroelectrics*, **221**, 157 (1999).
10. R.G. Batchko, V.Ya. Shur, M.M. Fejer, and R.L. Byer, *Appl. Phys. Lett.* (in press).
11. V.Ya. Shur and E.L. Rumyantsev, *Ferroelectrics*, **191**, 319 (1997)
12. V.Ya. Shur, *Phase Transitions*, **65**, 49 (1998).
13. E. Fatuzzo and W.J. Merz, *Ferroelectricity* (North-Holland, Amsterdam, 1967).
14. V.Ya. Shur, in *Ferroelectric Thin Films: Synthesis and Basic Properties*, **10,** eds. C.A. Paz de Araujo, J.F. Scott, G.W. Taylor (Gordon and Breach, New York, 1996), p.153.
15. P.V. Lambeck and G.H. Jonker, *Ferroelectrics*, **22**, 729 (1978).
16. V.M. Fridkin, *Ferroelectrics Semiconductors*, (Consult. Bureau, New York and London, 1980).
17. V.Ya. Shur, E.L. Rumyantsev, R.G. Batchko, G.D. Miller, M.M. Fejer, and R.L. Byer, *Phys. Solid State*, **41** (1999).
18. V. Gopalan and T.E. Mitchell, *J. Appl. Phys*., **85**, 2304, (1999).
19. V.Ya. Shur, E.L. Rumyantsev, E.V. Nikolaeva, E.I. Shishkin, R.G. Batchko, L.A. Eyres, M.M. Fejer, and R.L. Byer, *Phys. Rev. Lett.* (in press).
20. V.Ya. Shur, A.L. Gruverman, N.Yu. Ponomarev, and N.A. Tonkachyova, *Ferroelectrics*, **126**, 371 (1992).
21. R.G. Batchko, M.M. Fejer, R.L. Byer, D. Woll, R. Wallenstein, V.Ya. Shur, and L. Erman, *Optic Letters* (in press).